KSME

Springer

Journal of Mechanical Science and Technology 34 (3) 2020

Original Article
DOI 10.1007/s12206-020-0206-4

Keywords:
· Rolling bearing
· Fault detection
· Casing signal
· Minimum entropy deconvolution (MED)
· Variational mode decomposition (VMD)
· Filter size

Correspondence to:
Guo Chen
cgzyx@263.net

Citation:
He, Z., Chen, G., Hao, T., Teng, C., Hou, M., Cheng, Z. (2020). Weak fault detection method of rolling bearing based on testing signal far away from fault source. Journal of Mechanical Science and Technology 34 (3) (2020) ?~?. http://doi.org/10.1007/s12206-020-0206-4

Received September 11th, 2019
Revised December 1st, 2019
Accepted January 9th, 2020

† Recommended by Editor
No-cheol Park

Weak fault detection method of rolling bearing based on testing signal far away from fault source

Zhiyuan He[1], Guo Chen[1], Tengfei Hao[2], Chunyu Teng[3], Minli Hou[4] and Zhenjie Cheng[1]

[1]College of Civil Aviation, Nanjing University of Aeronautics and Astronautics, Nanjing 211106, China, [2]School of Automotive & Rail Transit, Nanjing Institute of Technology, Nanjing 211167, China, [3]Innovative Research Center, China Aero-Polytechnology Establishment, Beijing 100028, China, [4]Chengdu Aircraft Industrial (Group) Co. Ltd, Chengdu 610091, China

Abstract In some cases, because of the complex internal structure of the machines, the positions of the vibration sensors are far away from the rolling bearings, such as in an aero-engine, causing the fault features to become extremely weak, which brings great challenge to the detection of rolling bearings. To address this problem, an integrated detection method is proposed. First, a method named MEDL is proposed to determine the optimal filter length in minimum entropy deconvolution (MED) to enhance the periodic fault impulse component in the weak signal, which accuracy is 1. After that, the MEDL is combined with variational mode decomposition (VMD) and autocorrelation to extract fault features from strong background noise. A series of fault simulation experiments for rolling bearings were conducted by using an aero-engine rotor experimental rig with casing. The results verify that the accuracy of the integrated detection method is 100 % in different measuring points, speeds and fault types. At the same time, it compared with spectral kurtosis (SK) and empirical wavelet transform (EWT). It proves that the integrated detection method is more robust in extracting the weak fault characteristic of rolling bearings from the casing signals effectively.

1. Introduction

Rolling bearings are the core parts of important mechanical equipment, such as in aero-engines, wind turbines, automotive engines and so on, widely used in rotating machinery [1]. Monitoring of the running state of rolling bearings is essential. With the update of technology, bearing fault detection technology is gradually maturing. From the classical envelope analysis method [2] proposed at the earliest stage to the empirical mode decomposition (EMD) [3-5], wavelet analysis [6-8], and SK-based (spectral kurtosis) [9, 10] resonance band extraction methods, great success has been achieved, and these methods continue to be improved and updated [11-15].

When the bearing raceway is damaged, such as peeling, cracking, and pitting, impact vibration is usually generated when a rolling element passes, resulting in a series of periodic or quasi-periodic impacts. However, these impulses are subject to interference from other vibrational noises during the actual process, which makes them difficult to detect. Therefore, some researches focus on enhancing the impulse component in the signal, of which minimum entropy deconvolution (MED) [16] is a very effective method. Sawalhi et al. [17] first demonstrated its effectiveness when applied to bearings fault diagnosis. They combined the MED with the SK and achieved a remarkable result in enhancing the impulse component. Since then MED has become a common diagnostic method for bearings [18, 19]. However, some shortcomings still exist in the MED. It tends to maximize a single large random pulse, while the method of selecting the size of the filter is not clearly defined. Barszcz and Sawalhi [20] show that signal kurtosis value is proportional to the filter length, but there is no specific method to choose the filter length. Many studies rely on experience to select the filter length when using MED [19-21]. To

improve the shortcomings in MED, McDonald et al. proposed maximum correlated kurtosis deconvolution (MCKD) [22] and multipoint optimal minimum entropy deconvolution adjusted (MOMEDA) [23] methods successively. Their effectiveness is demonstrated by the gear fault signal. But there are many parameters in MCKD that need to be pre-set. So Miao [21] proposed a method of automatically selecting fault period to improve MCKD to solve this problem. Similarly, MOMEDA needs to pre-set a prior knowledge fault cycle, which increases the probability of misdiagnosis, and it can extract only one cycle pulse at a time. Later, some researchers made some improvements, such as optimizing the two parameters of cycle and filter size by using grasshopper optimization algorithm [24] and kurtosis spectral entropy [25]. Ref. [23] also expanded an algorithm called MED adjusted (MEDA) to solve the intermittent problem at the first sample point in the MED, but the filter size was still a problem. In addition, MEDA will lose some raw signal of the same length as the filter length.

Another aspect of signal processing, Dragomiretskiy and Zosso [26] proposed an adaptive signal decomposition method named variational mode decomposition (VMD), which is used to overcome the endpoint effect and modal-aliasing of EMD. It can adaptively decompose the signal into a certain number of sub-signals and has strong anti-noise ability. Many studies have proven that the VMD is better than the EMD-based methods in fault detection. For instance, Zhang et al. [27] used VMD to diagnose the fault signals of multistage centrifugal pump rolling bearings at different defects locations. The result of comparison the VMD and the EMD shows that the former is more outstanding. Wang et al. [28] applied VMD to extract the rub-impact fault features of the rotor system and demonstrated that the VMD has more fault signatures than the EMD and EWT. Satish et al. [29] extended a new bearing fault detection method based on VMD, correlation coefficient and Hurst index. Their analyses show that the VMD is superior in detecting faults than the EMD for acoustic signals. The performance of the VMD is affected by the parameters, so some have reported how to determine the parameters before decomposing the signal. For example, correlation coefficient and energy ratio are introduced in some papers [27, 30]. Bi et al. [31] combined with recursive model and energy difference tracking method to optimize the parameters. The optimized VMD can eliminate the influence of noise more accurately and quickly than the EMD. Gao et al. [32] employed the scale-space method to determine the number of the decomposed modes. Gong et al. [33] introduced a tentative VMD method and used dynamic time warping to determine the mode number adaptively for three bearing faults detection.

Note that vibration sensors cannot be located close to the bearings' position in some cases, such as in the aero-engine; generally, the signals are obtained from the aero-engine casing. Due to the complex structure of the machines, there are many vibration excitation sources and heavy noises, and the transmission paths cause the rolling bearing fault features weaker. Ref. [34] used an aero-engine rotor experimental rig whose structure is similar to a real aero-engine to simulate rolling bearing fault experiments. The vibration acceleration signals of the casing and the bearing housing were tested separately. The result shows that the effective fault signals from the fault vibration source transmitted from the casing attenuate nearly 80 %. Luo [35] proposed a new method called synchronous sampling technique combined with the envelope technique for aero-engine main bearing peeling detection. However, this method only validates the outer ring fault of rolling bearing, and damage detection of inner ring fault and rolling element fault has not been reported. And many researches for aero-engine rolling bearings lack a real aero-engine model with casing [36-39]. Obviously, in this case, it is necessary to research how to diagnose the fault features from weak signal far away from the bearing's position.

In this paper, an integrated detection method is proposed for weak fault features extraction of rolling bearings from the aero-engine rotor casing signal. First, a factor is introduced into the MED to select the appropriate filter length so as to get the optimal output signal. Then, modes of different frequency bands are separated by VMD and autocorrelation is used to eliminate the noise after that. Finally, the fault characteristic frequency is found in the envelope spectrum. Sec. 2, which is a review of MED, gives the details on how to choose the optimal filter length. The integrated detection method will be in Sec. 3. The rolling bearing fault experiments are introduced in Sec. 4. The weak fault features in the casing signal are analyzed, and the integrated detection method is verified in Sec. 5. Sec. 6 provides comparisons of the proposed method with the SK and EWT methods. Some conclusions are in Sec. 7

2. Optimal filter size selection for minimum entropy deconvolution

For linear systems $\vec{H}$, if we know the input $\vec{y}$, the output $\vec{x}$ can be expressed as:

$$\vec{x} = \vec{H} * \vec{y} \tag{1}$$

where $*$ is convolution operation. Blind deconvolution can be understood as finding the system $\vec{H}$ and input $\vec{y}$ in the case of only knowing the output $\vec{x}$. MED applies the principle of minimum entropy to the blind deconvolution problem. It is designed to maximize the kurtosis of the signal while suppressing noise components. It can be given by:

$$\vec{y} = \vec{f} * \vec{x} \tag{2}$$

$$\vec{y}=[y_1, y_2 \cdots y_N], \vec{f}=[f_1, f_2 \cdots f_L] \text{ and } \vec{x}=[x_1, x_2 \cdots x_N],$$

where N is the signal length, $\vec{f}$ is the finite impulse response filter. L is the filter length. The formula for calculating signal kurtosis is given by:

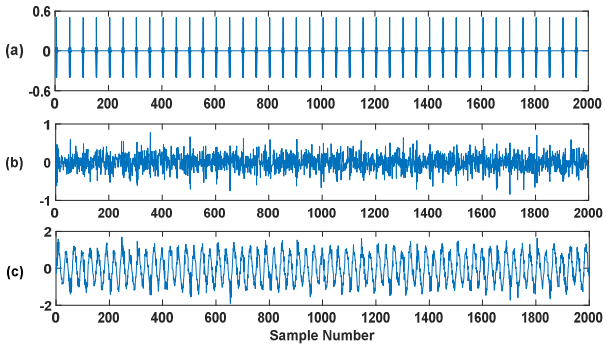

Fig. 1. The simulated fault signal: (a) The fault impulse component; (b) noise component with fault impulse; (c) the observed signal.

$$\text{kurt}=\frac{\sum_{n=1}^{N} y_n^4}{\left(\sum_{n=1}^{N} y_n^2\right)^2} . \tag{3}$$

Eq. (2) can be discretized and described as:

$$\vec{y}=\sum_{l=1}^{L} f_l x_{k-l+1} . \tag{4}$$

According to Ref. [16], the filter can be calculated by iteration:

$$\vec{f}=\frac{\sum_{n=1}^{N} y_n^2}{\sum_{n=1}^{N} y_n^4}\left(X_0 X_0^T\right)^{-1} X_0\left[y_1^3 y_2^3 \cdots y_N^3\right]^T , \tag{5}$$

where X_0 is:

$$X_0=\begin{bmatrix} x_1 & x_2 & x_3 & \cdots & \cdots & x_N \\ 0 & x_1 & x_2 & \cdots & \cdots & x_{N-1} \\ 0 & 0 & x_1 & \cdots & \cdots & x_{N-2} \\ \vdots & \vdots & \vdots & \ddots & \cdots & \vdots \\ 0 & 0 & 0 & \cdots & \cdots & x_{N-L+1} \end{bmatrix}_{L\times N} \tag{6}$$

The output result can be obtained by cyclical iteration. For more information, please refer to Ref. [21].

A simulation signal is established to illustrate the shortage of MED more intuitively in application to rotating machines fault detection. Let observed signal is:

$$x(t)=y(t)+n(t)+h(t) . \tag{7}$$

The signal consists of fault impulse component, noise and system harmonic. $y(t)$ represents the periodic impulse signal, and the fault interval is 50 sampling number as shown in Fig. 1(a). $n(t)$ represents the white Gaussian noise and mixed with the fault signal as shown in Fig. 1(b). The energy ratio of impulses to noise is 0.416. Fig. 1(c) is the observation signal $x(t)$, where:

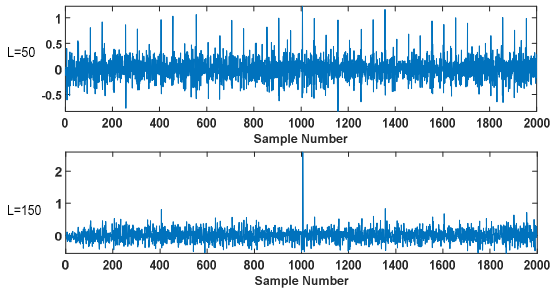

Fig. 2. The MED-filtered output signal at different filter lengths.

$$h(t)=0.1\sin(2\pi f_1 t)+0.2\sin(2\pi f_2 t)+\sin(2\pi f_3 t) \tag{8}$$

and $f_1=4f_2=2f_3=1/15$.

Fig. 2 plots the results of MED filtering $x(t)$ at the case of filter length L = 50 and L = 150. When L = 50, the periodic fault impulses can be seen in the output though accompanied with heavy noise interference. However, the situation is different at L = 150, MED only extracted a large single pulse, which is not the output we want. For rotating machinery, raising the periodic pulses from the weak signal is the key to detection. Therefore, it is imperative to determine the optimal filter length before using the MED.

In this paper, an energy factor L_μ is proposed in MED. It can be described as:

$$L_\mu=\frac{\sum_{n=1}^{N} y_{nL}^2}{\sum_{n=1}^{N}\left(x_n-y_{nL}\right)^2} , \tag{9}$$

where N is the raw signal point x_n is the raw signal. y_{nL} is the output whose filter length is L. When the output signal approaches the periodic pulse signal, the kurtosis of the continuous weak impulse signal is maximized by the filter. Therefore, the amplitude of the output signal on the time domain waveform is relatively large, and the system harmonics and noise are suppressed at this moment, so the energy ratio of the output signal to the residual signal appears to be a larger value. Conversely, when the output signal is a single pulse, except for the impact characteristic of the larger amplitude at a certain time in the time domain waveform, the remaining part is the noise component and the output signal is less differentiated from the system harmonic noise; L_μ will behave as a smaller value. So the optimal filter length can be determined by calculating the value of L_μ.

Before calculating L_μ, the range of L should be given. For example in the simulated signal $x(t)$, Fig. 3 plots the kurtosis and L_μ of the MED-filtered output signal from L=0 to L=500. Fig. 3(a) shows that the larger the filter size the larger the kurtosis. This is consistent with the results of Ref. [20]. It is not hard to comprehend because MED aims to maximize the kurtosis. However, it is not feasible to select the filter length only by virtue of the kurtosis information of the signal, because the change in kurtosis is not related to whether the output signal is

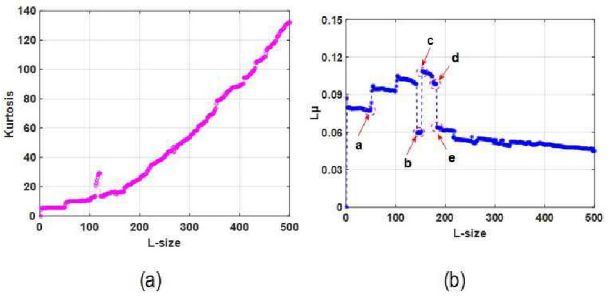

Fig. 3. (a) The kurtosis of the output signal; (b) L_μ of output signal at different filter size.

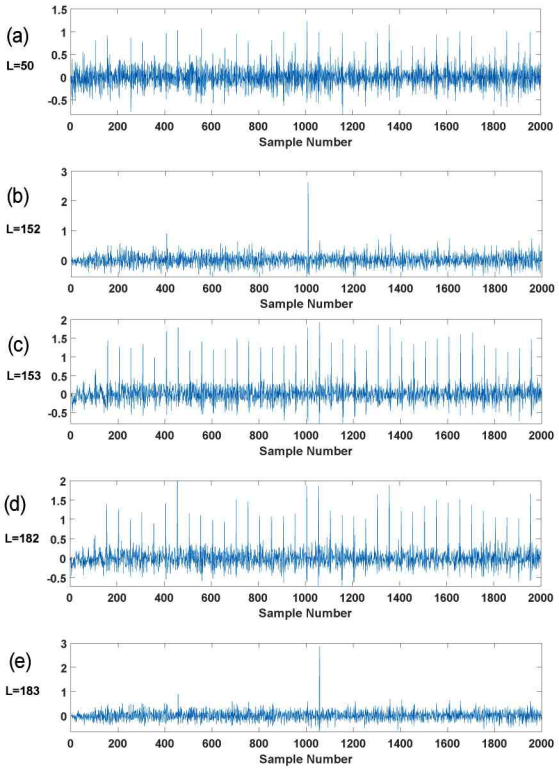

Fig. 4. The MED-filtered output signals at different filter lengths.

the continuous impulses. The trend of L_μ is in Fig. 3(b). At point c, L_μ has the highest value, and the values of b and e are very low. The filter lengths of five points in Fig. 3(b) are 50, 152, 153, 182 and 183. The results of their MED-filtered output signals are shown in Fig. 4.

It can be seen that the larger the L_μ, the better the periodic impulse recovering effect. Compared with a, the outputs of c and d have less noise, and the periodic fault impulses are more conspicuous. But in the cases of points b and e, the outputs are even worse. It is remarkable that the difference between the filter length values of b (d) and c (e) is just 1, but their outputs are entirely different, which indicates that the selection of filter size L is a critical step in the MED. To achieve the best MED-filtered output, the filter length with maximum L_μ will be considered as the optimal filter length. This method is named

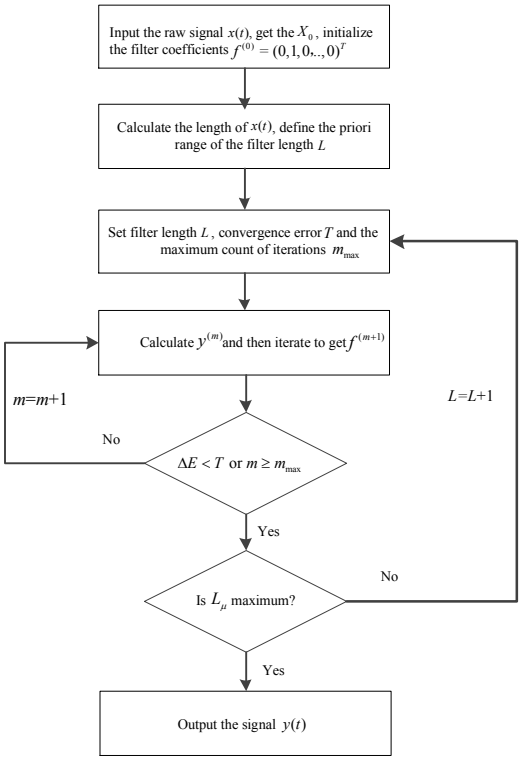

Fig. 5. Flowchart of the MEDL method.

as MEDL in this paper, whose specific flow paths (Fig. 5) are as follows:

(1) Initialize $f^{(0)}=(0,1,0,..,0)^T$ meanwhile input the raw signal $x(t)$ to get X_0.

(2) Calculate the length of $x(t)$ and define the priori range of the filter length L. Set convergence error T and the maximum count of iterations $m_{\max}$.

(3) According to Eq. (4), calculate $y^{(m)}$ by substituting X_0 and filter coefficient $f^{(m)}$, then get the $f^{(m+1)}$ by Eq. (5).

(4) Calculate the error $\Delta E=\left|O_4(f^{(m+1)})-O_4(f^{(m)})\right|$, $O_4(\cdot)$ represents the result of Eq. (3).

(5) If $m<m_{\max}$ and $\Delta E<T$, continue cyclic iteration from step (3), otherwise, calculate L_μ.

(6) Output the signal $y(t)$ when L_μ reach maximum.

3. The integrated fault detection method

3.1 Review of VMD

Variational mode decomposition (VMD) mainly includes two processes, establishing and solving the variational model. A real signal is non-recursively decomposed into the sub-signals pattern u_k with discrete number K. The aim of optimization is to minimize the bandwidth of each mode. The unilateral spectrum of u_k can be calculated by:

$$\left(\delta(t)+\frac{j}{\pi t}\right)*u_k(t), \tag{10}$$

where $\delta(t)$ is Dirac delta function. The whole spectrum of each modal component is translated to the predicted central frequency by multiplying the signal $e^{-j\omega_k t}$,where ω_k is the estimated center frequency, it is expressed as follows:

$$\left[\left(\delta(t)+\frac{j}{\pi t}\right)*u_k(t)\right]e^{-j\omega_k t}. \tag{11}$$

The constraint variation problem is thus constructed as follows:

$$\begin{aligned}&\min_{\{u_k\},\{\omega_k\}}\left\{\sum_k\left\|\partial_t\left[\left(\delta(t)+\frac{j}{\pi t}\right)*u_k(t)\right]e^{-j\omega_k t}\right\|_2^2\right\}\\&\text{subject to}\sum_k u_k=f\end{aligned} \tag{12}$$

where $\{u_k\}=\{u_1,\cdots,u_k\}$ and $\{\omega_k\}=\{\omega_1,\cdots,\omega_k\}$.

The quadratic penalty factor α and the Lagrange multiplication operator $\lambda(t)$ are introduced to solve the Eq. (12) minimization problem:

$$\begin{aligned}L(\{u_k\},\{\omega_k\},\lambda)=&\alpha\sum_k\left\|\partial_t\left[\left(\delta(t)+\frac{j}{\pi t}\right)*u_k(t)\right]e^{-j\omega_k t}\right\|_2^2\\&+\left\|f(t)-\sum_k u_k(t)\right\|_2^2+\left\langle\lambda(t),f(t)-\sum_k u_k(t)\right\rangle\end{aligned} \tag{13}$$

Eq. (13) can be solved by the alternate direction method of multipliers ADMM, and by searching for u_k^{n+1}, ω_k^{n+1} and λ_k^{n+1} alternately. From the Ref. [26]:

$$\hat{u}_k^{n+1}(\omega)=\frac{\hat{f}(\omega)-\sum_{i\neq k}\hat{u}_i(\omega)+\frac{\hat{\lambda}(\omega)}{2}}{1+2\alpha(\omega-\omega_k)^2}. \tag{14}$$

Similarly, the central frequency constrained variational problem can be constructed, and the center frequency can be finally obtained:

$$\omega_k^{n+1}=\frac{\int_0^\infty\omega\left|\hat{u}_k(\omega)\right|^2d\omega}{\int_0^\infty\left|\hat{u}_k(\omega)\right|^2d\omega}. \tag{15}$$

The iterative algorithm of VMD is as follows:

(1) Initialize $\{\hat{u}_k^1\}$, $\{\hat{\omega}_k^1\}$, $\{\hat{\lambda}_k^1\}$ and n ;

(2) According to Eqs. (14) and (15), get and update u_k and ω_k;

(3) λ_k^{n+1} can be updated by:

$$\hat{\lambda}^{n+1}(\omega)\leftarrow\hat{\lambda}^n(\omega)+\tau\left[\hat{f}(\omega)-\sum_k\hat{u}_k^{n+1}(\omega)\right];$$

(4) if $\sum_k\left\|\hat{u}_k^{n+1}-\hat{u}_k^n\right\|_2^2/\left\|\hat{u}_k^n\right\|_2^2<\varepsilon$ stop and get the output, otherwise go back to step (2).

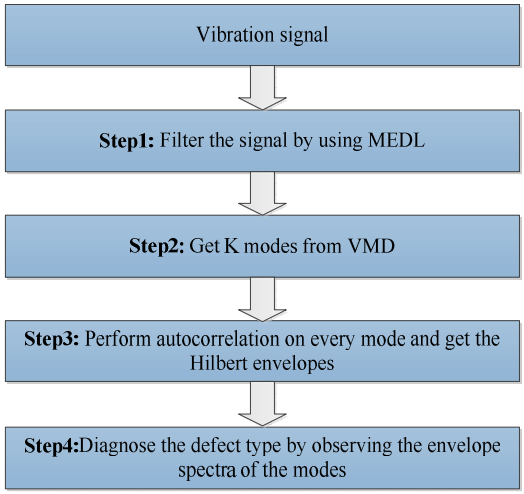

Fig. 6. Steps of the integrated detection method.

3.2 The steps of integrated diagnosis method

To extract the fault characteristics from the weak signal far away from the vibration source, an integrated detection method which combines MEDL, VMD and autocorrelation is proposed. Specific steps are as follows:

Step 1 : MEDL filters the raw signal and obtains the output signal. At the optimal filter length, MEDL can fully enhance the fault pulses in the raw signal, thereby eliminating the interference of the transmission path and noise.

Step 2 : The MEDL-filtered output signal is decomposed into K sub-signals by VMD. These modes have different frequency bands, which is helpful to find the resonance frequency band of fault bearing. The parameters K and α in the VMD are determined by energy ratio and correlation method. It will be introduced in the Sec. 5.

Step 3 : Autocorrelation processing is performed on each sub-signal, and K envelope spectra are obtained. Autocorrelation has a good performance in removing the aperiodic noise, so that the periodic component in the sub-signal can be retained.

Step 4 : The defect type is diagnosed by observing the envelope spectra to determine whether the corresponding fault characteristic frequency exists.

4. Experiment

4.1 Aero-engine rotor experimental rig

To simulate the condition that the rolling bearing is far away from the sensors, an aero-engine rotor experimental rig is used. The rotor experimental rig is very close to a real aero-engine, which has a single rotor. Its typical features are as follows: (1) It has a multi-segment casing with a ratio of 1:3 to the real engine and its shape is similar to a real aero-engine; (2) The internal

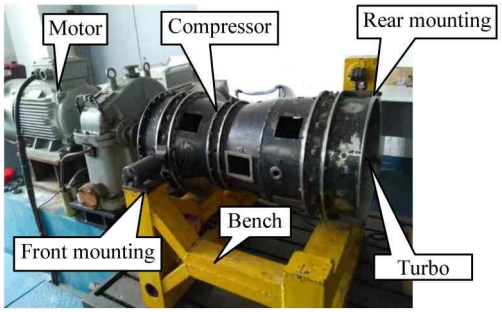

(a)

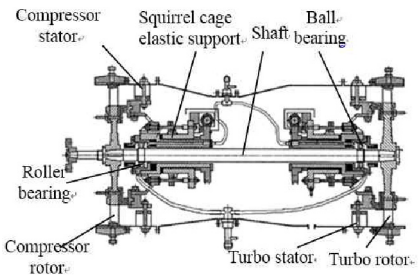

(b)

Fig. 7. Aero-engine rotor experimental rig: (a) Rotor; (b) structure.

(a) (b) (c)

Fig. 8. Fault 6206 ball bearings used in the experiment.

structure is simplified, and the rotor support structure is 0-2-0. Two discs with blades represent the compressor disk and the turbine disk, respectively, and two bearings are supported between them. The outsides of the two disks have no bearing. (3) The elastic support structure is adopted, and the support stiffness can be adjusted to change the dynamics system. (4) The rotor without combustion chamber structure is driven by the motor.

4.2 Artificial fault ball bearings

Faulty 6206 ball bearings (see Fig. 8) were installed on the turbine support. The defects were artificially seeded on the outer race, inner race and ball, respectively. The three kinds of faulty bearings were processed by machine tool wire cutting to produce cracks. These cracks on the outer race and the inner race are both 0.6 mm width and 0.5 mm depth. And the crack on the ball is rough 1 mm diameter with 2 mm depth.

The vibration signals were acquired from casing measuring point and the bearing housing measuring point, respectively, as shown in Fig. 9. There are two B&K4805 ICP acceleration sensors respectively placed on the vertical and horizontal direction of the casing, one sensor on the bearing housing, whose sampling rate is 10.24 kHz. The data acquisition card is NI-USB9234 and each data is 8192 points. The 6206 ball bearing main dimensions are shown in Table 1. Formulas for calculating the fault characteristic frequencies are given in Table 2. The rotating speeds are 1500 rpm, 1800 rpm, 2000 rpm, and 2400 rpm.

Table 1. 6206 fault bearing dimensions (unit: mm).

Pitch diameter D	Thickness	Diameter of ball d	Ball number Z	Contact angle ϕ
46	16	9.5	9	0

Table 2. Characteristic frequencies of rolling bearing faults.

Fault type	Calculation formula
BPFO	$\frac{Z}{2} f_r \left(1-\frac{d}{D}\cos\phi\right)$
BPFI	$\frac{Z}{2} f_r \left(1+\frac{d}{D}\cos\phi\right)$
BSF	$\frac{D}{2d}\left\{1-\left(\frac{d}{D}\cos\phi\right)^2\right\}$

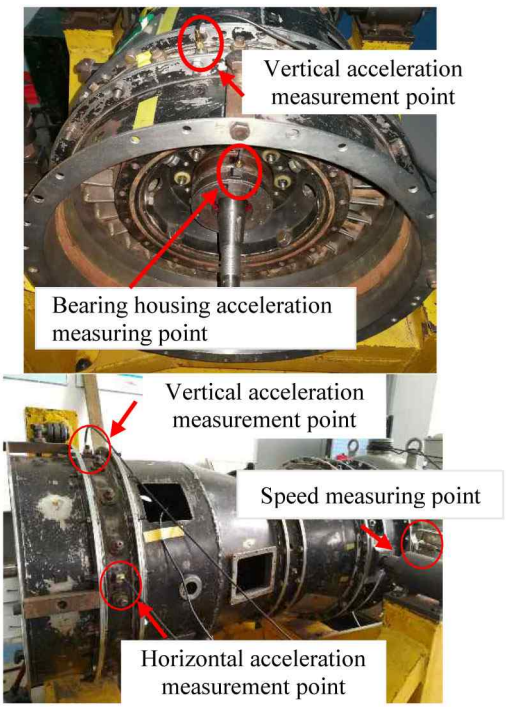

Fig. 9. The location of sensors.

4.3 Weak fault features in the casing signal

In Sec. 4.2, four rotating speeds were carried out. Given the limited space available, we selected 1800 rpm (other results are presented in Table 3) as an example to verify the practicability of the integrated detection method. Fig. 10 shows the

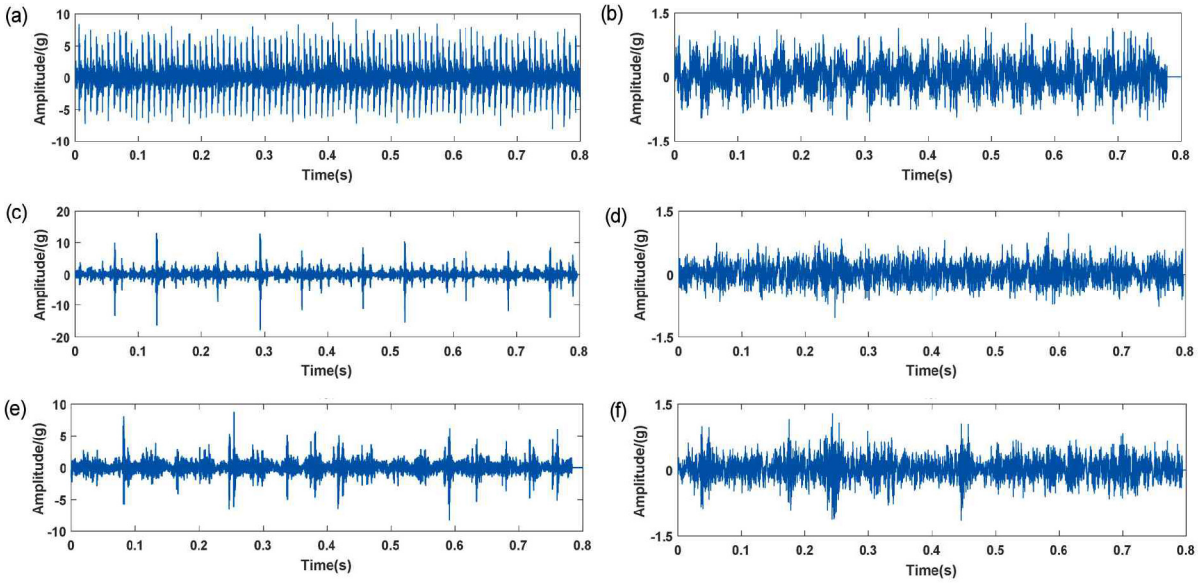

Fig. 10. Time-domain waveforms of different faults: (a) Outer race fault; (c) inner race fault; (e) ball fault from the bearing housing; (b) outer race fault; (d) inner race fault; (f) ball fault from the horizontal point of the casing.

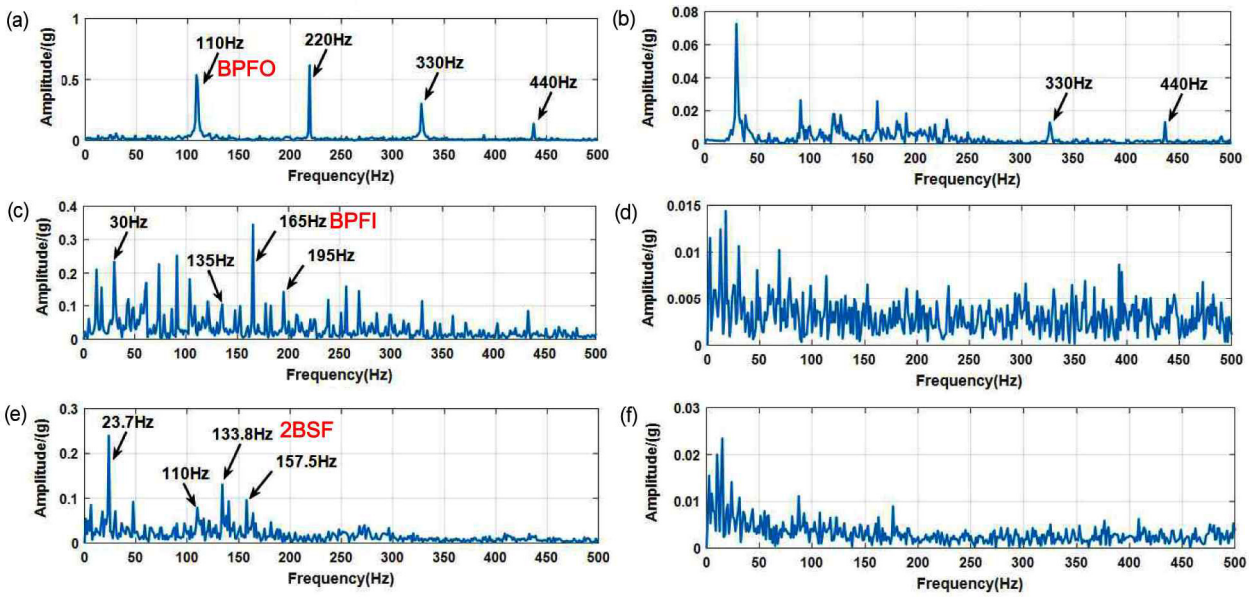

Fig. 11. Envelope spectra of different faults: (a) Outer race fault; (c) inner race fault; (e) ball fault from the bearing housing; (b) outer race fault; (d) inner race fault; (f) ball fault from the horizontal point of the casing.

time-domain waveforms of three failure modes at 1800 rpm. Figs. 10(a), (c) and (e) are collected from the bearing housing, while Figs. 10(b), (d) and (f) from the horizontal measurement point on the casing. Obviously, it can be seen that the fault signals of bearing housing have a clear impact and large amplitude, but the impulses in casing signals are covered by a large amount of noise. There are few consecutive fault impulses in the time domain waveforms.

Fig. 11 draws the envelope spectra of the signals. As can be seen from Fig. 11(a), BPFO is 110 Hz, and its harmonics are particularly obvious, but in its corresponding casing signal, Fig. 11(b), BPFO has only a few weak harmonic components. Similarly, in Fig. 11(c), BPFI exhibits 165 Hz, and with the rotor rotational modulation frequencies 135 Hz and 195 Hz. However, in the result of casing signal, Fig. 11(d), there is no BPFI, just some noisy frequencies. The same is true in the analysis of ball fault. Note that the even harmonics of BSF are often dominant, in particular in envelope spectrum [1], and with cage modulation frequencies. So the fault feature on the ball is 133.8 Hz, and 23.7 Hz is the second harmonic of cage rotation

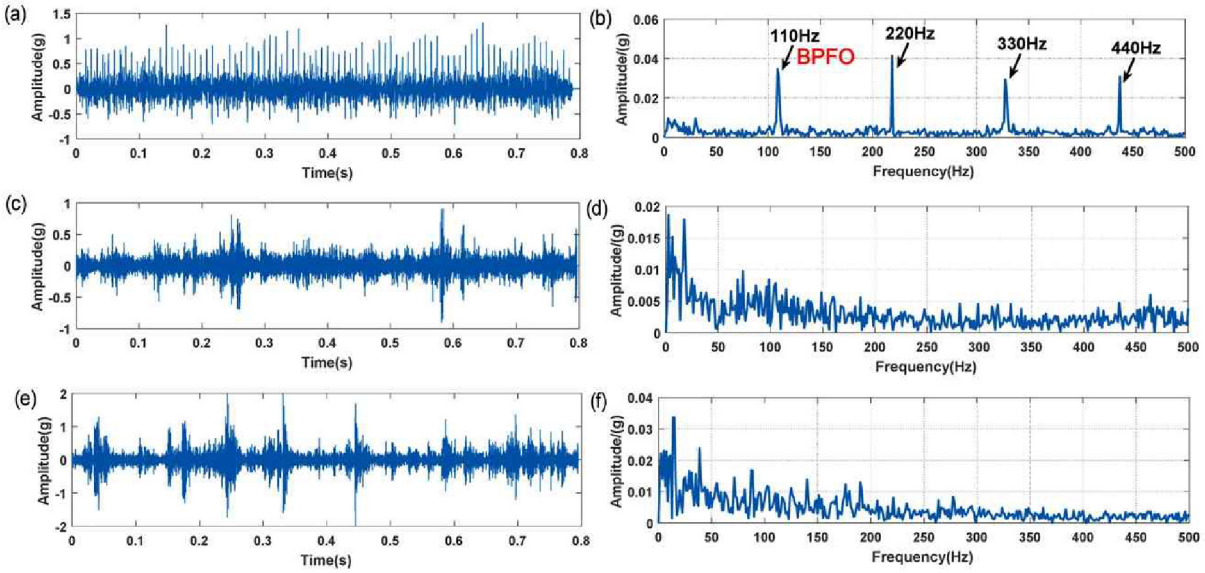

Fig. 12. The MEDL-filtered outputs of the horizontal casing signals: (a) Outer race fault; (b) envelope of (a); (c) inner race fault; (d) envelope of (c); (e) ball fault; (f) envelope of (e).

frequency which appears as the modulation frequency in Fig. 11(e). According to the above results, the fault characteristics in the casing signal attenuate seriously due to the transmission of the path.

5. The verification of integrated detection method

Sec. 4.3 shows that the fault features in the casing signal are very weak. Next, based on the envelope spectrum analysis, the MEDL, VMD and integrated detection method are used to detect the casing signal, respectively, to compare the effect of the single method to reflect the superiority of the integrated detection method.

5.1 Detecting casing signal with MEDL

It has been demonstrated that MEDL can enhance periodic impulses in noisy signal at optimal filter lengths in Sec. 2. So MEDL was applied to the horizontal casing signals, respectively. The results of MEDL-filtered outputs are shown in Fig. 12. The optimal filter length of Fig. 12(a) is 108. Fig. 12(a) shows that the periodic impulses are obvious and the BPFO in Fig. 12(b) is also prominent. So MEDL successfully recovers the fault information of outer race. However, as for inner race fault in Fig. 12(c) and ball fault in Fig. 12(e), the optimal filter lengths are 28 and 14. Although large impulse components can be observed in MEDL-filtered outputs, the fault characteristic frequencies cannot be found in their envelope spectra from Figs. 12(d) and (e), because the inner fault and ball fault have speed modulation in the process of rotation, and they are seriously disturbed by noise. In this case, using MEDL alone does not meet the detection requirements of inner race fault and ball fault.

5.2 Detecting casing signal with VMD

Before applying VMD to decompose the signal, it necessary to predefine the parameters K and α. it may lose useful information if K is too small. On the contrary, big K will give rise to worthless components which bring about wasting computing resource. Parameter α affects the precision of the signal. Therefore, we use the energy ratio and correlation method to select the parameters [27]. The energy ratio and correlation are defined as:

$$E_{XY} = \frac{\sum_{i=1}^{N}(X_i)^2}{\sum_{i=1}^{N}(Y_i)^2}, \tag{16}$$

$$C_{XY} = \frac{\sum_{i=1}^{N}(X_i - \bar{X})(Y_i - \bar{Y})}{\sqrt{\sum_{i=1}^{N}(X_i - \bar{X})^2}\sqrt{\sum_{i=1}^{N}(Y_i - \bar{Y})^2}}, \tag{17}$$

where N is the data length, $\bar{X} = \frac{1}{N}\sum_{i=1}^{N} X_i$, $\bar{Y} = \frac{1}{N}\sum_{i=1}^{N} Y_i$.

At 1800 rpm, the energy ratio and correlation between the sub-signals and the raw signals from bearing housing are shown in Fig. 13. The energy ratio is the sum of the ratios of all modes. The maximum energy mode is selected to calculate the correlation. Here, default parameter α = 2000 is used first to determine K, and then parameter α is corrected according to K. As can be seen from Fig. 13(a). the energy ratio increases when K<7 and then tends to be stable, which means the signal has been fully decomposed when K increases to a certain value. In Fig. 13(b), the correlation shows a step-down trend. After K = 8, the correlation gradually decreases and tends to be stable. Figs. 13(c) and (d) reflect the effect of α on the energy ratio and correlation. When α < 500, the energy

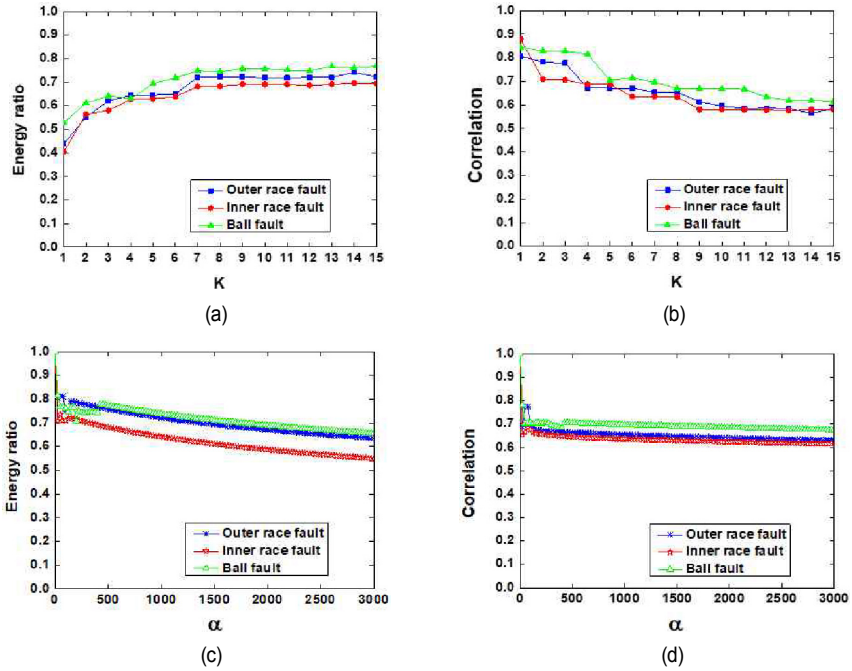

Fig. 13. Variation of energy ratio and correlation for different fault bearing housing signals decomposed under different parameters: (a) and (b) Energy ratio and correlation with different K; (c) and (d) energy ratio and correlation with different α.

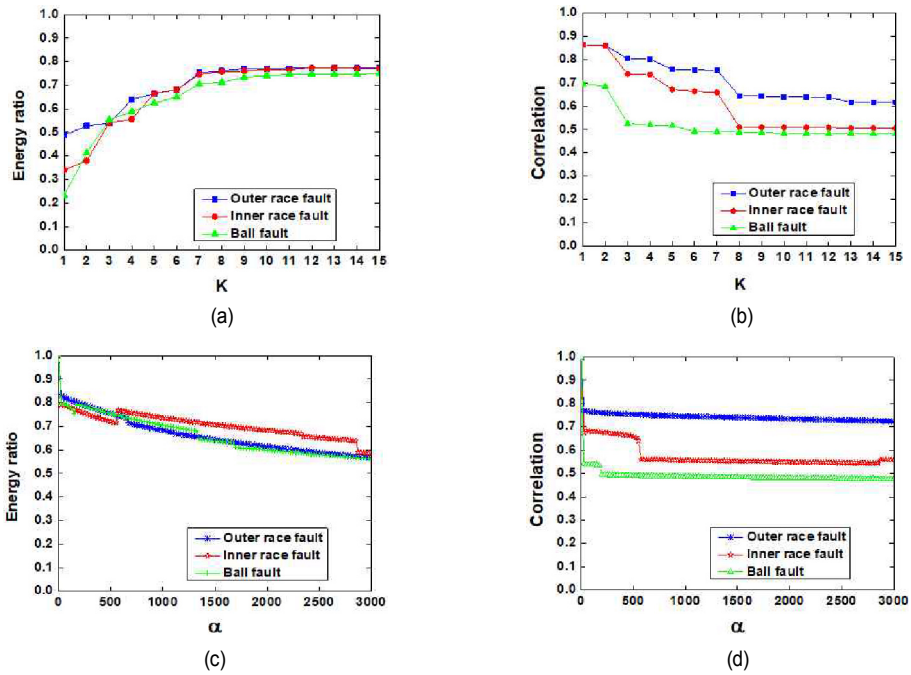

Fig. 14. Variation of energy ratio and correlation for different fault casing signals decomposed under different parameters: (a) and (b) Energy ratio and correlation with different K; (c) and (d) energy ratio and correlation with different α.

ratio and correlation fluctuate slightly and then show a stable state, and the energy ratio slowly decreases. Similarly, for the horizontal casing signals at 1800 rpm, the variation trend of parameters is similar to the result of bearing housing signal. To make sure the signal can be decomposed adequately and make the modes have the highest correlation as far as possible, we chose K = 7, α = 1000.

The inner race fault horizontal casing signal (Fig. 10(d)) and ball fault (Fig. 10(f)) casing signal were decomposed by VMD. The optimal result was selected by observing the envelope spectra from the seven sub-signals. The results are printed in Fig. 15. As can be seen in Fig. 15(a) there is only a suspicious

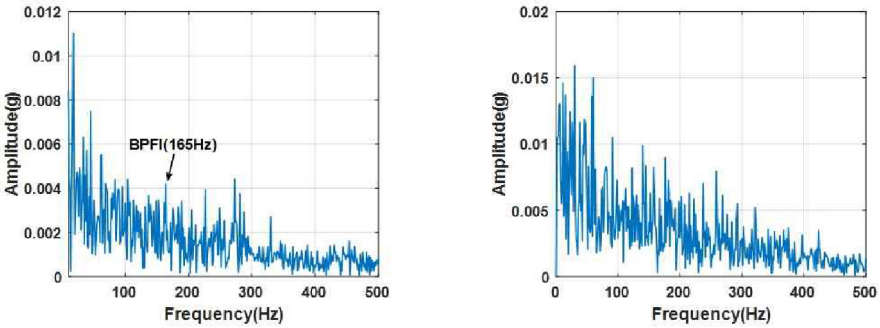

Fig. 15. The result of horizontal case signal by VMD: (a) Inner race fault; (b) ball fault.

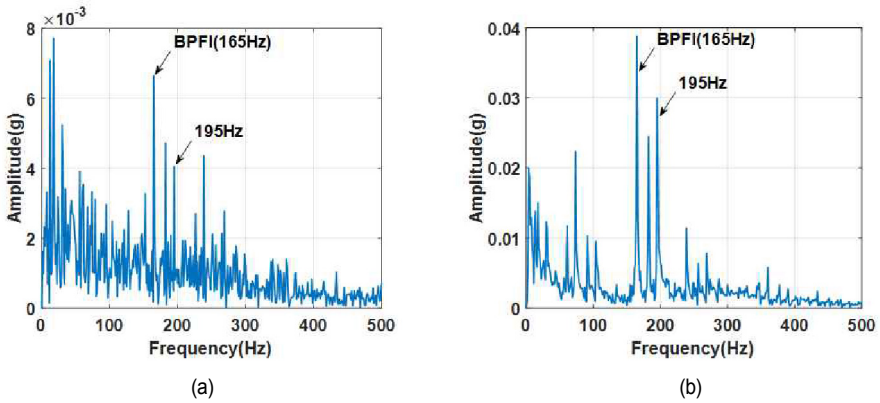

Fig. 16. The envelope spectrum of the horizontal casing signal for inner race fault: (a) The result of MEDL+VMD; (b) the result of the integrated detection method.

weak BPFI in the envelope spectrum with heavy noise. Meanwhile, there is no ball fault characteristic frequency in the envelope spectrum either in Fig. 15(b). In the casing signals without MEDL filtering, the fault pulses covered by noise are very weak, which is not conducive to finding the resonance band by VMD. Obviously, just using the VMD method cannot identify the fault characteristics of the horizontal casing signal.

5.3 Detecting casing signal with integrated detection method

To solve the problem of extracting weak features, MEDL is used to enhance the impulses and then VMD is performed. Fig. 16(a) shows the result of inner race fault, where the BPFI (165 Hz) is obvious, and the rotational modulation frequency also appears on the right side, but there are still some noises. To remove them to get maximum benefit, autocorrelation is applied after MEDL+VMD, namely, integrated detection method. The result in Fig. 16(b) shows that not only is the fault characteristic frequency greatly improved, but also the noises are almost eliminated, and the modulation phenomenon of inner race fault is clearly compared with Fig. 16(a). As for rolling element fault, it can be clearly seen the fault characteristic frequency in the envelope spectra in Fig. 17. Integrated detection method can give more prominence to fault characteristic frequency in Fig. 17(b). Analysis above suggests that the proposed method is successful. Although weak information cannot be captured by VMD alone, the enhancement of impulses after MEDL is beneficial to the separation of resonance band and noise. Finally, autocorrelation clears noise away.

6. Comparing the integrated detection method with other methods

6.1 Compared with the MED+SK+SES

Spectral kurtosis (SK) method is a classical method in bearing diagnosis. Refs. [17, 19] proposed a method which combines the MED, SK and squared envelope spectrum (SES) to detect the bearings, proving that it is very effective in detecting weak faults. Formally, it is similar to the integrated detection method. So MED+SK+SES is used to detect the horizontal casing signals to compare with the integrated detection method.

Fig. 18 plots the result of inner race fault. To make it fair, the filter size is the same as before. The frequency band in Fig. 18(a) with the highest kurtosis is 4480 Hz and the bandwidth is 1280 Hz in level 2, but in its squared envelope spectrum, Fig. 18(b), there is no BPFI. The situation in the result of rolling element fault is not better than inner race fault. The frequency

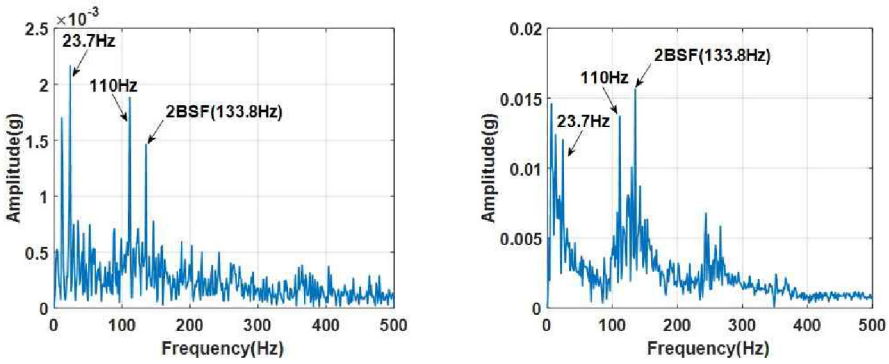

Fig. 17. The envelope spectrum of the horizontal casing signal for ball fault: (a) The result of MEDL+VMD; (b) the result of the integrated detection method.

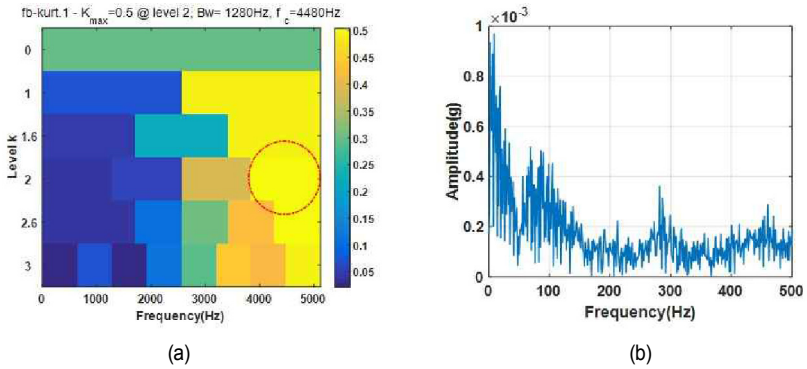

Fig. 18. The result of MED+SK+SES for the inner race fault of horizontal casing signal: (a) Kurtogram; (b) the squared envelope spectrum.

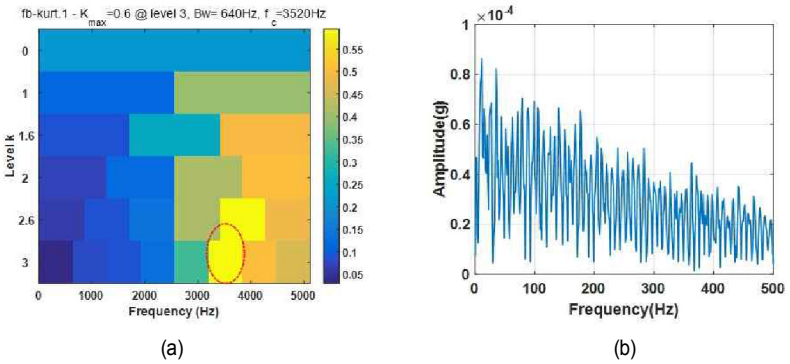

Fig. 19. The result of MED+SK+SES for the ball fault of horizontal casing signal: (a) Kurtogram; (b) the squared envelope spectrum.

band in Fig. 19(a) with the highest kurtosis is 3520 Hz, and the bandwidth is 640 Hz in level 3. In the squared envelope spectrum as shown in Fig. 19(b), there are no frequency components associated with fault characteristics. SK method is very sensitive to the impact of large kurtosis. After using MED, the impacts in the signals are improved, but from Figs. 12(c) and (e) there are still some large interference noises. SK method can easily locate the resonance frequency band to the interference noise. So the results are not satisfactory. Therefore, the diagnostic effects of MED+SK+SES are not good when the sensors are away from the bearing.

6.2 Compared with EWT

Empirical wavelet transform (EWT) [40] as a new method also has good performance for signal decomposition, and it has proven to be very effective in detecting the fault features of rolling bearings [41]. As for integrated detection method, for the same casing signal, if other steps change nothing but replace the VMD method with the EWT method in the step 2, we can compare the applicability of the two integrated detection methods. In this part, we used the EWT method provided in Ref. [40] for comparison. For more detailed process of EWT, please

Table 3. Comparison of two integrated detection method.

Rotating speed/rpm	Vertical measuring point						Horizontal measuring point					
	Inner race fault		Outer race fault		Ball fault		Inner race fault		Outer race fault		Ball fault	
	VMD	EWT	VMD	EWT	VMD	EWT	VMD	EWT	VMD	EWT	VMD	EWT
1500	G	N	G	G	N	N	G	N	G	G	N	B
	137 Hz		92 Hz		118 Hz		136 Hz		91 Hz		118 Hz	
1800	N	B	G	G	N	N	G	G	G	G	G	B
	165 Hz		108 Hz		136 Hz		165 Hz		110 Hz		134 Hz	
2000	G	N	G	G	G	B	G	B	G	G	G	B
	182 Hz		120 Hz		156 Hz		182 Hz		121 Hz		156 Hz	
2400	G	N	G	G	G	B	G	N	G	G	N	B
	220 Hz		144 Hz		181 Hz		220 Hz		143 Hz		183 Hz	

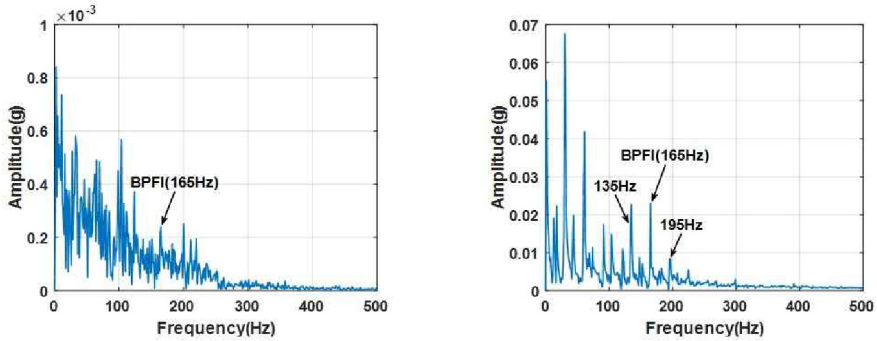

(a) (b)

Fig. 20. The envelope spectrum of the horizontal casing signal for inner race fault: (a) The result of MEDL+EWT; (b) the result of EWT integrated detection method.

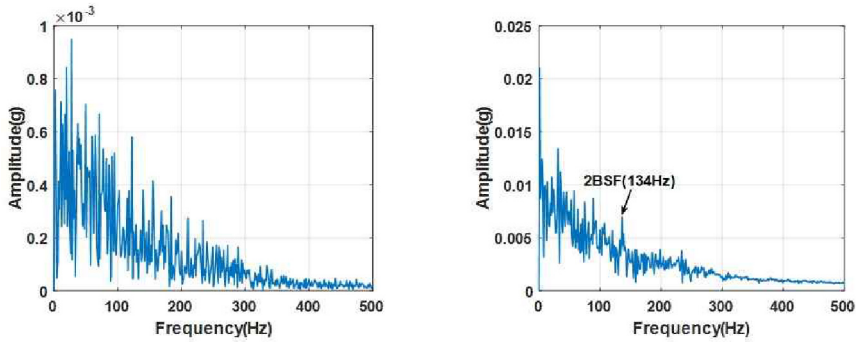

(a) (b)

Fig. 21. The envelope spectrum of the horizontal casing signal for inner race fault: (a) The result of MEDL+EWT; (b) the result of EWT integrated detection method.

refer to it.

Similarly, selecting horizontal casing signal at 1800 rpm, Fig. 20(a) plots the spectrum of MEDL+EWT for inner race fault. It presents a weak BPFI; after autocorrelation in Fig. 20(b), the situation has improved. In the spectrum, BPFI is clear as well as the rotational modulation frequencies, but the result of VMD integrated detection method in Fig. 16(b) is better. However, for ball fault, the fault characteristic frequency is inconspicuous, whether in Fig. 21(a) or Fig. 21(b). Obviously, the VMD integrated detection method is superior to EWT integrated detection method in extracting weak fault features.

Table 3 gives the result of two integrated detection method for different fault at all test rotating speeds. The diagnostic effect is divided into Good (**G**), which represents that the bearing fault characteristic frequency can be significant highlighted, for example, Fig. 16(b); Normal: **(N)**, indicating that the bearing fault characteristic frequency can be clearly seen, but the result is not as good as '**G**' grade, such as Fig. 20(b); Bad: (**B**), indicating the fault feature cannot be found, such as Fig. 21(b).

Table 3 illustrates that VMD integrated detection method can extract fault features in almost all cases, while EWT integrated detection method loses its detection ability in the case of ball failure, which indicates that VMD integrated detection method has excellent performance in extracting weak faults from the

signal far away from the fault source.

7. Conclusions

In this paper, an integrated detection method is proposed for weak fault features extraction of rolling bearings from casing signals which combines MEDL, VMD and autocorrelation methods. It enhances the impulse component of weak signals, removing irrelevant interference components, and makes full use of the decomposition ability of VMD. Three different faults are successfully detected from the casing signal. It can be summarized as follows:

(1) The fault experiments of rolling bearings were simulated by an aero-engine rotor experimental rig at different rotating speeds. The transmission path weakens the fault features in the casing signals.

(2) To avoid the problem of enhancing single impulse in MED, a factor L_μ is proposed to determine the optimal filter length, which aims to maximize periodic fault impulses. The MEDL is verified by the simulation signal, and MEDL can enhance the weak fault impulses in the casing signals and successfully extract the fault characteristics of the outer race fault, but it fails in the situations of the inner race fault and the ball fault. Just using VMD method cannot identify the fault characteristics of the casing signal, either.

(3) Compared with integrated detection method, the results show that the MED+SK+SES method cannot extract the weak fault information when the sensors are far away from the bearing. Besides, EWT integrated detection method is used for comparison, but it fails to extract ball fault feature in most cases.

It is noteworthy that parameters need to be predetermined in the integrated detection method. In this work, the selection of VMD parameters has not been automated. Therefore, In the following work it is necessary to study parameter auto-optimized method to achieve fast integrated diagnosis.

Acknowledgments

The authors thank professor Michael Pecht for his advice on this paper. This work is supported by the National Natural Science Foundation of China (No. 51675263) and National Science and Technology Major Project (2017IV00080045). We are also grateful to the teachers and students who have helped in the experiment. We would like to share our experiments with interested researchers at http://ides.nuaa.edu.cn/ides/index.asp.

References

[1] R. B. Randall and J. Antoni, Rolling element bearing diagnostics - A tutorial, *Mechanical Systems and Signal Processing*, 25 (2) (2011) 485-520.

[2] M. S. Darlow, R. H. Badgley and G. W. Hogg, *Application of High Frequency Resonance Techniques for Bearing Diagnostics in Helicopter Gearboxes*, Technical Report, US Army Air Mobility Research and Development Laboratory (1974) 74-77.

[3] N. E. Huang, Z. Shen, S. R. Long, M. C. Wu, H. H. Shih, Q. Zheng, N.-C. Yen, C. C. Tung and H. H. Liu, The empirical mode decomposition and the Hilbert spectrum for nonlinear and non-stationary time series analysis, *Proceedings of the Royal Society A*, 454 (1971) (1998) 903-995.

[4] H. Li, Y. Zhang and H. Zheng, Hilbert-Huang transform and marginal spectrum for detection and diagnosis of localized defects in roller bearings, *J. of Mechanical Science and Technology,* 23 (2) (2009) 291-301.

[5] D. Hongbo, K. Qi, X. Chen, Y. Zi, Z. He and B. Li, Sifting process of EMD and its application in rolling element bearing fault diagnosis, *J. of Mechanical Science and Technology,* 23 (8) (2009) 2000-2007.

[6] W. Dong, M. Qiang, F. Xianfeng and H. Hongzhong, Rolling element bearing fault detection using an improved combination of Hilbert and wavelet transforms, *J. of Mechanical Science and Technology,* 23 (12) (2009) 3292-3301.

[7] H. Li, L. Fu and H. Zheng, Bearing fault diagnosis based on amplitude and phase map of Hermitian wavelet transform, *J. of Mechanical Science and Technology*, 25 (11) (2011) 2731-2740.

[8] J. D. Wu and C. C. Hsu, Fault gear identification using vibration signal with discrete wavelet transform technique and fuzzy-logic inference, *Expert Systems with Applications*, 36 (2-part-P2) (2009) 3785-3794.

[9] J. Antoni and R. B. Randall, The spectral kurtosis application to the vibratory surveillance and diagnostics of rotating machines, *Mechanical Systems and Signal Processing,* 20 (2) (2006) 308-331.

[10] J. Antoni, Fast computation of the kurtogram for the detection of transient faults, *Mechanical Systems and Signal Processing,* 21 (1) (2007) 108-124.

[11] Y. T. Sheen, An envelope analysis based on the resonance modes of the mechanical system for the bearing defect diagnosis, *Measurement,* 43 (7) (2010) 912-934.

[12] Q. Xiong, Y. Xu, Y. Peng, W. Zhang, Y. Li and L. Tang, Low-speed rolling bearing fault diagnosis based on EMD denoising and parameter estimate with alpha stable distribution, *J. of Mechanical Science and Technology*, 31 (4) (2017) 1587-1601.

[13] S. Wan and B. Peng, The FERgram: A rolling bearing compound fault diagnosis based on maximal overlap discrete wavelet packet transform and fault energy ratio, *J. of Mechanical Science and Technology,* 33 (1) (2019) 157-172.

[14] S. Wan, X. Zhang and L. Dou, Compound fault diagnosis of bearings using improved fast spectral kurtosis with VMD, *J. of Mechanical Science and Technology,* 32 (2018) 5189.

[15] A. Moshrefzadeh and A. Fasana, The autogram: An effective approach for selecting the optimal demodulation band in rolling element bearings diagnosis, *Mechanical Systems and Signal Processing*, 105 (2018) 294-318.

[16] R. Wiggins, A minimum entropy deconvolution, *Geoexploration*, 16 (1-2) (1978) 21-35.

[17] N. Sawalhi, R. B. Randall and H. Endo, The enhancement of fault detection and diagnosis in rolling element bearings using minimum entropy deconvolution combined with spectral kurtosis, *Mechanical Systems and Signal Processing*, 21 (6) (2007) 2616-2633.

[18] C. Yao, Z. Ning, W. Zhang and Z. Wang, Application of an improved minimum entropy deconvolution method for railway rolling element bearing fault diagnosis, *J. of Sound and Vibration,* 425 (2018) 53-69.

[19] M. E. Abboud, W. A. Smith and R. B. Randall, Advanced bearing diagnostics A comparative study of two powerful approaches, *Mechanical Systems and Signal Processing,* 114 (2019) 604-627.

[20] T. Barszcz and N. Sawalhi, Fault detection enhancement in rolling element bearings using the minimum entropy deconvolution, *Archives of Acoustics*, 37 (2) (2012) 131-141.

[21] M. Yonghao, M. Zhao, J. Lin and Y. Lei, Application of an improved maximum correlated kurtosis deconvolution method for fault diagnosis of rolling element bearings, *Mechanical Systems and Signal Processing,* 92 (2017) 173-195.

[22] G. L. Mcdonald, Q. Zhao and M. J. Zuo, Maximum correlated Kurtosis deconvolution and application on gear tooth chip fault detection, *Mechanical Systems and Signal Processing*, 33 (2012) 237-255.

[23] G. L. Mcdonald and Q. Zhao, Multipoint optimal minimum entropy deconvolution and convolution fix: Application to vibration fault detection, *Mechanical Systems and Signal Processing,* 82 (2016) 461-477.

[24] C. J. Zhou, J. Ma, J. Wu and Z. Feng, A parameter adaptive MOMEDA method based on grasshopper optimization algorithm to extract fault features, *Mathematical Problems in Engineering* (2019) 22.

[25] Z. Wang, W. Du, J. Wang, J. Zhou, X. Han, Z. Ziying and L. Huang, Research and application of improved adaptive MOMEDA fault diagnosis method, *Measurement,* 140 (2019) 63-75.

[26] K. Dragomiretskiy and D. Zosso, Variational mode decomposition, *IEEE Transactions on Signal Processing,* 62 (3) (2014) 531-544.

[27] M. Zhang, Z. Jiang and K. Feng, Research on variational mode decomposition in rolling bearings fault diagnosis of the multistage centrifugal pump, *Mechanical Systems and Signal Processing,* 93 (2017) 460-493.

[28] Y. Wang, R. Markert, J. Xiang and W. Zheng, Research on variational mode decomposition and its application in detecting rub-impact fault of the rotor system, *Mechanical Systems and Signal Processing,* 60-61 (2015) 243-251.

[29] S. Mohanty, K. K. Gupta and K. S. Raju, Hurst based vibro-acoustic feature extraction of bearing using EMD and VMD, *Measurement,* 117 (2018) 200-220.

[30] J. Xingxing, J. Wang, J. Shi, C. Shen, W. Huang and Z. Zhu, A coarse-to-fine decomposing strategy of VMD for extraction of weak repetitive transients in fault diagnosis of rotating machines, *Mechanical Systems and Signal Processing,* 116 (2019) 668-692.

[31] F. Bi, X. Li, C. Liu, C. Tian, T. Ma and X. Yang, Knock detection based on the optimized variational mode decomposition, *Measurement,* 140 (2019) 1-13.

[32] Z. Gao, X. Wang, J. Lin and Y. Liao, Online evaluation of metal burn degrees based on acoustic emission and variational mode decomposition, *Measurement,* 103 (2017) 302-310.

[33] T. K. Gong, X. H. Yuan, Y. B. Yuan, X. H. Lei and X. Wang, Application of tentative variational mode decomposition in fault feature detection of rolling element bearing, *Measurement,* 135 (2019) 481-492.

[34] G. Chen, T. F. Hao and H. F. Wang, Sensitivity analysis and experimental research on ball bearing early fault diagnosis based on testing signal from casing, *J. of Dynamic Systems, Measurement, and Control,* 136 (6) (2014) 061009.

[35] H. Luo, H. Qiu, G. Ghanime, M. Hirz and G. van der Merwe, Synthesized synchronous sampling technique for bearing damage detection preprint, *J. of Engineering for Gas Turbines & Power,* 132 (7) (2009) 072501.

[36] M. Yu, Z. Feng, J. Huang and Y. Yu, Characteristic extraction of ball bearing compound faults of aero-engine, *J. of Vibroengineering*, 19 (6) (2007) 4285 4299.

[37] Z. Han, D. Zhaohui and F. Zuowei, Sparse decomposition based aero-engine's bearing fault diagnosis, Jixie Gongcheng Xuebao*, J. of Mechanical Engineering*, 51 (1) (2015) 97-105.

[38] H. Lin, Z. Wu, K. Xue and Y. Guoan, Research on aero-engine bearing fault using acoustic emission technique based on wavelet packet decomposition and support vector machine, *2017 IEEE 2nd Advanced Information Technology, Electronic and Automation Control Conference (IAEAC) IEEE* (2017*).*

[39] A.-B. Ming, W. Zhang, H. He, X. Yu and F. Chu, Incipient fault feature extraction of main bearing by iterative squared envelope analysis, *Prognostics & System Health Management Conference IEEE* (2017*).*

[40] J. Gilles, Empirical wavelet transform, *IEEE Transactions on Signal Processing,* 61 (16) (2013) 3999-4010.

[41] M. Kedadouche, M. Thomas and A. Tahan, A comparative study between empirical wavelet transforms and empirical mode decomposition methods: Application to bearing defect diagnosis, *Mechanical Systems and Signal Processing,* 81 (2016) 88-107.

Zhiyuan He received his B.S. from Nanjing University of Aeronautics and Astronautics, Nanjing, P. R. China, in 2017. Now he is a Ph.D. student in the College of Civil Aviation, Nanjing University of Aeronautics and Astronautics, Nanjing, P. R. China. His current research interests include rotating-machine fault diagnosis, signal analysis and processing.

Guo Chen received a Ph.D. in Mechanical Engineering from the Southwest Jiaotong University, Chengdu, P. R. China, in 2000. Now he works at the College of Civil Aviation, Nanjing University of Aeronautics and Astronautics, Nanjing, P. R. China. His current research interests include the whole aero-engine vibration, rotor-bearing dynamics, rotating-machine fault diagnosis, signal analysis and processing, et al.